JTTEE5 18:536–545
DOI: 10.1007/s11666-009-9339-9
1059-9630/$19.00 © ASM International

FeAl and $NbAl_3$ Intermetallic-HVOF Coatings: Structure and Properties

J.M. Guilemany, N. Cinca, S. Dosta, and I.G. Cano

(Submitted September 9, 2008; in revised form March 25, 2009)

Transition metal aluminides in their coating form are currently being explored in terms of resistance to oxidation and mechanical behavior. This interest in transition metal aluminides is mainly due to the fact that their high Al content makes them attractive for high-temperature applications. This is also a reason to study their resistance to wear; they may be suitable for use in applications that produce a lot of wear in aggressive environments, thus replacing established coating materials. In this study, the microstructure, microhardness, and wear and oxidation performance of FeAl and $NbAl_3$ coatings produced by high-velocity oxy-fuel spraying are evaluated with two main aims: (i) to compare these two coating systems—a commonly studied aluminide (FeAl) and, $NbAl_3$, an aluminide whose deposition by thermal spraying has not been attempted to date—and (ii) to analyze the relationship between their microstructure, composition and properties, and so clarify their wear and oxidation mechanisms. In the present study, the higher hardness of niobium aluminide coatings did not correlate with a higher wear resistance and, finally, although pesting phenomena (disintegration in oxidizing environments) were already known of in bulk niobium aluminides, here their behavior in the coating form is examined. It was shown that such accelerated oxidation was inevitable with respect to the better resistance of FeAl, but further improvements are foreseen by addition of alloying elements in that alloy.

Keywords friction and wear, corrosion of HVOF coatings, high temperature oxidation, wear and corrosion

1. Introduction

In recent decades, the challenge of using transition metal aluminides for structural applications has been approached in many different ways. These aluminides are called advanced materials due to their possible use in high-temperature applications with light-weight benefits and reasonably good strengths (Ref 1). Important advantages, such as high melting points, high strength-to-weight ratios and excellent resistance to hostile environments, mean that attention has been focused on nickel-, iron-, and titanium-based aluminides (Ref 2-4). The main shortcoming of these materials, however, is their poor ductility, which is improved either by changing the processing routes (Ref 5-8) or by the addition of ternary elements (Ref 2, 9-14). This lack of toughness is one of the reasons why they are good candidates for use as coatings. Moreover, regarding their high aluminum levels, it would not be possible to manufacture structural components with good load-carrying capabilities; therefore, they can be used as oxidation resistant coatings allowing the use of a substrate material with improved mechanical properties.

J.M. Guilemany, N. Cinca, S. Dosta, and **I.G. Cano**, Centre de Projecció Tèrmica (CPT). Universitat de Barcelona, Martí i Franquès 1, 08028 Barcelona, Spain. Contact e-mail: nuria.cinca@ub.edu.

Current research into these compounds in bulk form is mainly focused on their brittleness and high-temperature behavior; moreover, few wear-related studies have been undertaken until that moment. In the early 1970s, a variety of aluminide and silicide coatings were applied to steel substrates to protect them from oxidation. Aluminides were the first choices for low-temperature environments or short thermal cycles. In the literature, however, only structural properties are reported and few characterization results for the hardness and wear performance of thermally sprayed coatings are given.

Materials for high-temperature applications can broadly be divided into two categories: those used to replace Ni-based superalloys, with significant reductions in density (this is where Fe-, Ni-, and Ti-aluminides might be included) and a second category of materials whose high-temperature characteristics are more useful than those of superalloys (>1100 °C). It is as part of this second category that $NbAl_3$ has recently been studied. In the present study, the results obtained for iron aluminide coatings (microstructure, hardness, wear, and oxidation resistance) are reviewed and these are compared with those for a niobium aluminide coating. The Fe-Al system is fairly well understood and Fe_3Al and FeAl based alloys are proposed for commercial use. Commercially available Grade 3 Fe40Al powder was selected for this study because it has nearly 50% Al content and a nanocrystalline structure. Within the Nb-Al system, there are crystalline structures that are much more complex than that of FeAl, which is of the CsCl-type. This leads to higher melting points and, thus, more affordable temperature efficiencies (Ref 15). However, catastrophic oxidation behavior is exhibited by the compound with the highest Al content ($NbAl_3$) as a

result of the phenomenon known as ''pesting.'' This has been of great concern since the early studies of niobium alloys appeared as a result of developments in the aircraft engine industry. Specifically, much of the development was within the context of the growing space program. In the late 1960s and mid-1970s, research into high-strength niobium alloys was increased. The most promising mixtures were those with alloying elements such as Hf, W, or Ta (Ref 16). However, Hebda already reported in his review (Ref 16) that there was little optimism as to the practical use of niobium alloys for long-life turbojet engines, because of the unreliability of their coating and the inaccessibility of internal components for frequent inspection to detect coating disintegration. Ways around this problem have been searched for by some authors and, despite being still at the preliminary stage, some success has been reported by recent studies into nanocrystallization (Ref 17). This is why there is still interest in a coating with improved life and higher temperature resistance, but no strong demand for higher-temperature niobium alloys.

These are, therefore, two very different aluminides; thus, the main purpose of the present study is twofold: optimize thermal spray conditions for production of HVOF FeAl and $NbAl_3$ coatings and, correlate their microstructures with their mechanical and oxidation properties. Among the several thermal spray methods, HVOF was employed as a way of reducing the oxidation of the powder particles during their time within the flame and of producing dense coatings with the highest possible amount of intermetallic phase.

2. Experimental Procedure

FeAl and $NbAl_3$ feedstock powders were supplied by CEA-DTEN (Grenoble) and ABSCO Ltd., respectively. The former is Grade 3 (atomized and ball-milled) with a nominal composition of Fe-40Al-0.05 Zr (at.%) with 50 ppm B and 1 wt.% Y_2O_3, while the latter is the alloy obtained by mechanical alloying. Their particle size distribution was studied by means of a laser diffraction particle size analyzer BECKMAN COULTER LS and their flowability was measured according to the ASTM B-213-30 standard. These powders were sprayed onto low-alloy carbon steel specimens.

A Diamond Jet Hybrid (DJH2700) from SULZER METCO was used to produce the coatings, with the thermal spray parameters reported in Table 1. $NbAl_3$ powder was preheated before spraying to improve its flow through the nozzle. The powders and the as-sprayed coatings were examined by scanning electron microscopy (JEOL 5510) operated at 20 kV with a coupled EDS system. The XRD analyses were performed in a Bragg-Brentano θ/2θ Siemens D-500 diffractometer with a graphite monochromator using Cu $K\alpha$ radiation.

Table 1 Thermal spraying parameters

	FeAl	$NbAl_3$
Oxygen flow rate, L/min	180-190	250-260
Propylene flow rate, L/min	80-90	70-80
Carrier gas, L/min	300-310	370-380
Oxygen/fuel ratio	2.8	4.2
Feeding rate, g/min	20	15
Spraying distance, mm	250	240

For the Vickers micro-indentation tests, Matsuzawa MXT-α equipment with a normal load of 200 gf was used. At least 10 measurements were performed on each sample and the mean value calculated.

Wear resistance was evaluated by a ball-on-disk test (ASTM G99-03) and a rubber-wheel test (ASTM G65-00) for the sliding friction and abrasive effects, respectively. In the former test, the sliding counterpart was a ∅11 mm WC-Co ball that was slid over the polished sample with a circular track of 16 mm up to a distance of 1000 m and with an applied normal load of 5 N. The rotating rubber wheel was moved at a constant 139 rpm on the specimen, while silica particles were allowed to flow under the influence of gravity between the two surfaces. A normal load of 50 N was applied and the mass loss was measured for 30 min. The friction wear rate ($mm^3\ N^{-1}\ m^{-1}$) was calculated from the volume loss obtained by means of white light interferometry (SWLI) using a surface analysis microscope (Zygo New View 100); the abrasive wear rate was calculated from the mass loss per test time.

Finally, oxidation behavior was assessed in two ways. First, the oxidation kinetics were tested through thermogravimetric measurements carried out for small pieces of debonded coatings, under continuous air flow in TA Instruments SDT 2960 DSC-TGA equipment with a heating rate of 10 °C/min. The isothermal tests were carried out for 72 h at 500 and 900 °C to explore behavior at moderate and high temperatures. Second, to examine the performance of as-sprayed deposits (coated specimens), these were placed in a furnace under oxidizing conditions and left for 72 h at the same temperatures (500 and 900 °C). Furthermore, as it was already known that oxidation damage is caused by pesting, a set of samples was tested for 1 h under oxidizing and low-oxidizing conditions (with Ar flux) in order to clarify what happens at early stages of oxidation.

3. Results and Discussion

3.1 Feedstock Powder Characterization

Figure 1 shows the morphology, particle size distribution, and x-ray scan of Fe40Al powder; it has an angular shape (Fig. 1a) as a result of the milling process. As has already been discussed in other studies in which such a powder has been used, the milling step serves two purposes. First, intense plastic deformation induces nanocrystallization within the structure, as can be seen from the broad x-ray peaks (Fig. 1c) and second, the addition of yttria was intended to reinforce the grain boundaries. Figure 1(b) shows the homogeneous particle size distribution, with d_{90} below 30 μm; this suggested the particles would be suitable for spraying because of their flowability.

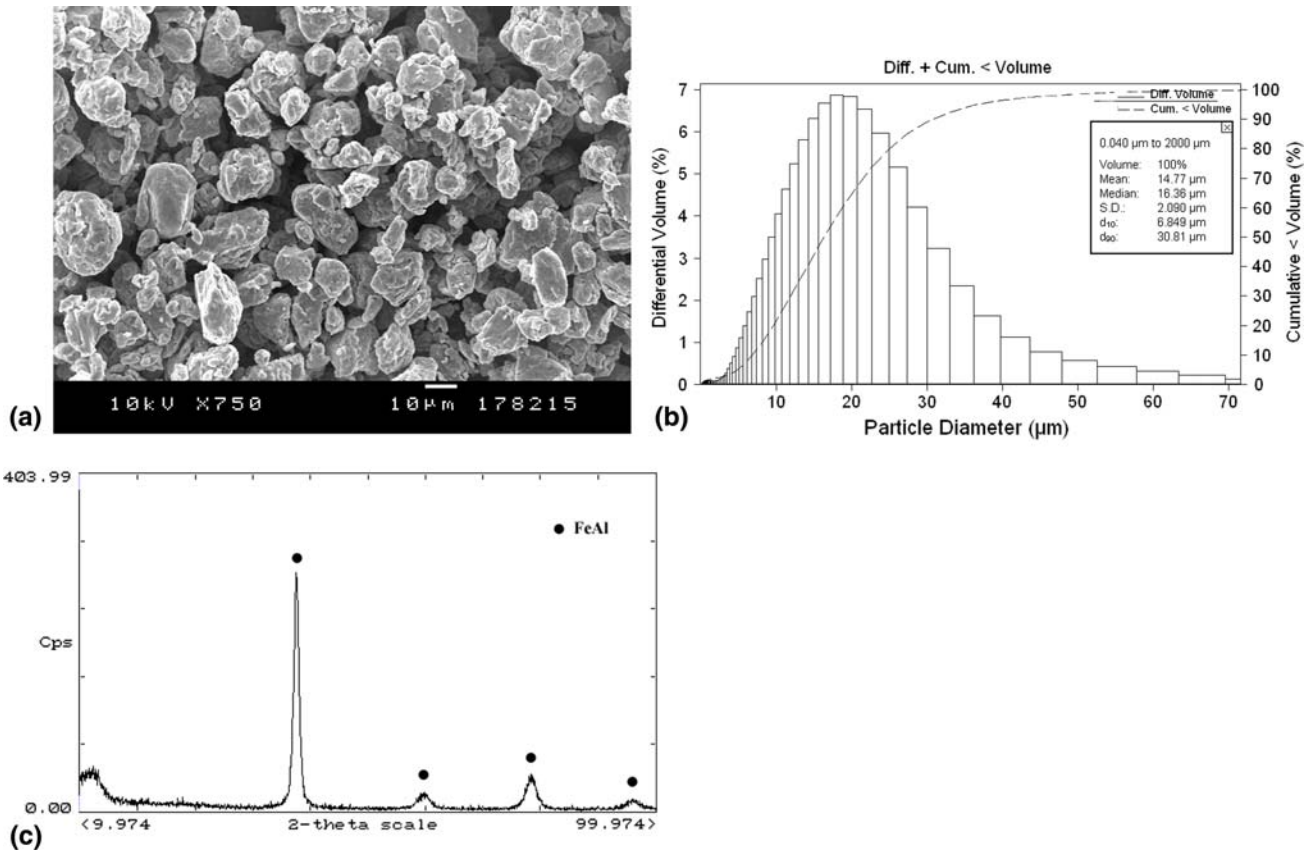

Fig. 1 (a) Morphology, (b) particle size distribution, and (c) x-ray scan of the Fe40at.%Al powder

Figure 2(a-c) shows the morphology, particle size distribution, and x-ray scan of the niobium aluminide powder, respectively. An initial examination at low magnification showed that there was a wide range of particle sizes. Some are as large as 50 µm in diameter, but there are also very small particles that tend to agglomerate. According to the particle size plot, a very broad distribution was found for the $NbAl_3$ powder. As could be expected from this, the powder showed no fluidity at all, which would lead to many difficulties for spraying. The x-ray trace shows that it is predominantly formed of the $NbAl_3$ phase, with a trace of Nb_2Al.

3.2 Coating Microstructures

The characteristics of the Fe40Al coating have been discussed in detail elsewhere (Ref 18). It can be seen from Fig. 3(a) that it consists of a homogeneous and quite dense coating with good adherence and intersplat cohesion. At high magnification, the microstructure features a light and dark gray pattern associated with the intermetallic phase and oxidation (Fig. 3b). Oxide phases are mainly encountered at the splat boundaries as a result of particle oxidation during in-flight time; some light contrasts also indicate that these areas are depleted in Al (Fe-rich zones). The x-ray scan shows an intermetallic phase as well as the spinel $FeAl_2O_4$ oxide (Fig. 3c). While the initial powder showed only the characteristic lines of a B2 lattice ($h+k+l=$ even), indicating that it had a disordered structure, the spraying process leads to the appearance of superlattice lines ($h+k+l=$ odd) (Ref 19). Since the process of milling the initial pre-alloy (atomized) powder disordered the crystal lattice, the ordering effect associated with the appearance of superlattice lines after spraying could be ascribed to the high temperatures, which made the rearrangement of the atoms possible to some extent. However, Al depletion, as well as the partial melting of particle cores, prevents the formation of an ordered B2 structure.

Although the $NbAl_3$ powder was heated prior to spraying, the nozzle was often blocked, making it difficult for a uniform coating to be produced. However, a 92 ± 5 µm-thick deposit was achieved (Fig. 4a). Figure 4(b) shows its microstructure with characteristic lamellas (fully melted particles), surrounded by open porosity; the dark and light gray areas correspond to oxidized and Nb-rich zones, according to EDS microanalysis. The XRD indicates the presence of $NbAl_3$, NbO, NbO_2, and Al_2O_3 (Fig. 4c). For both the iron and niobium aluminides, propylene was used as fuel; however, the considerably lower oxygen/fuel ratio for the iron aluminide coating left much more fuel unused, which served to cool the particles during the spraying process. These conditions also helped to minimize the oxide content.

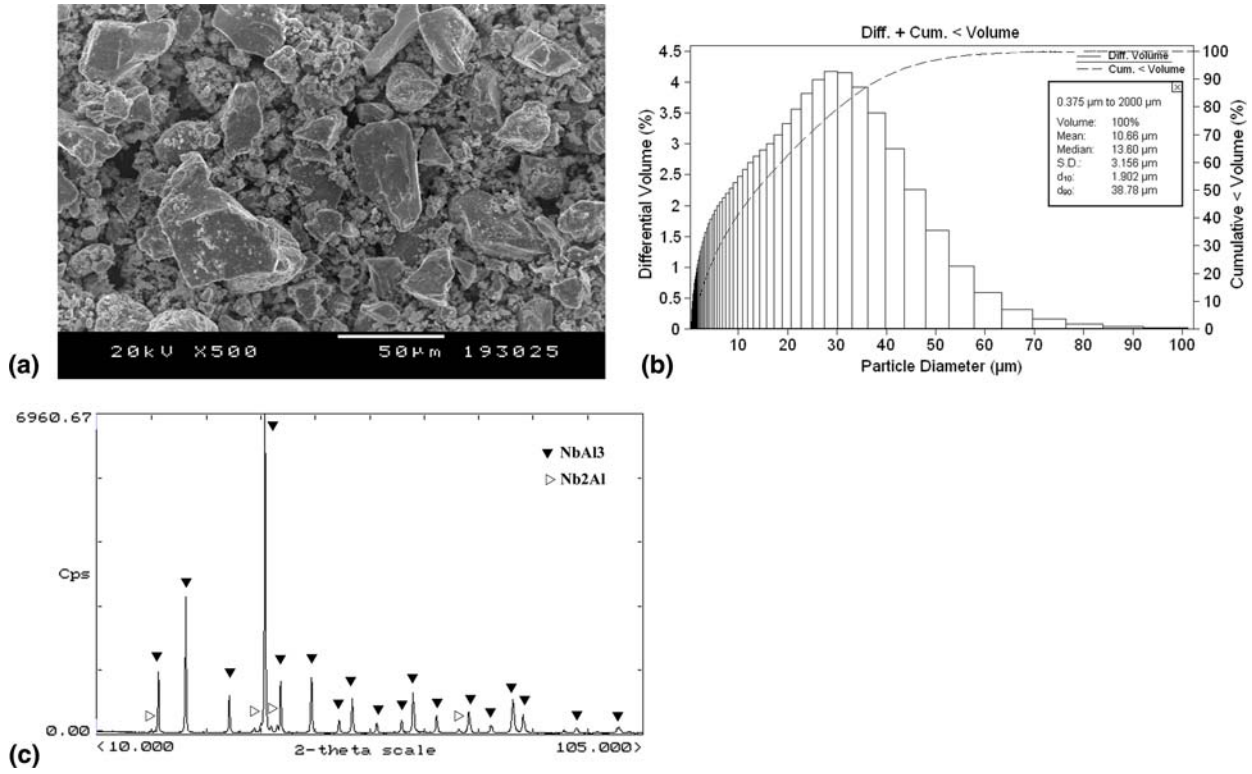

Fig. 2 (a) Morphology, (b) particle size distribution, and (c) x-ray scan of the $NbAl_3$ powder

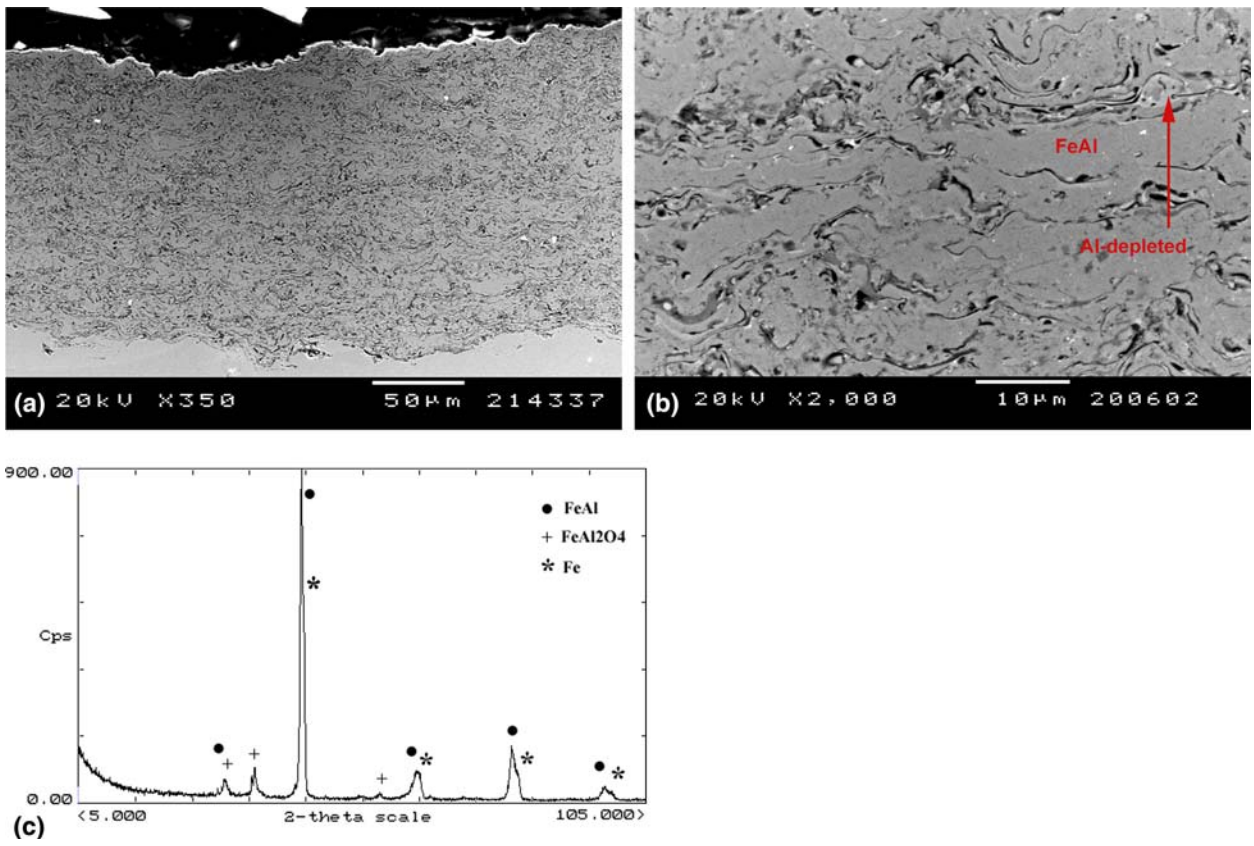

Fig. 3 (a) General view and (b) magnification of the as-sprayed cross section Fe40Al coating, and (c) x-ray spectrum

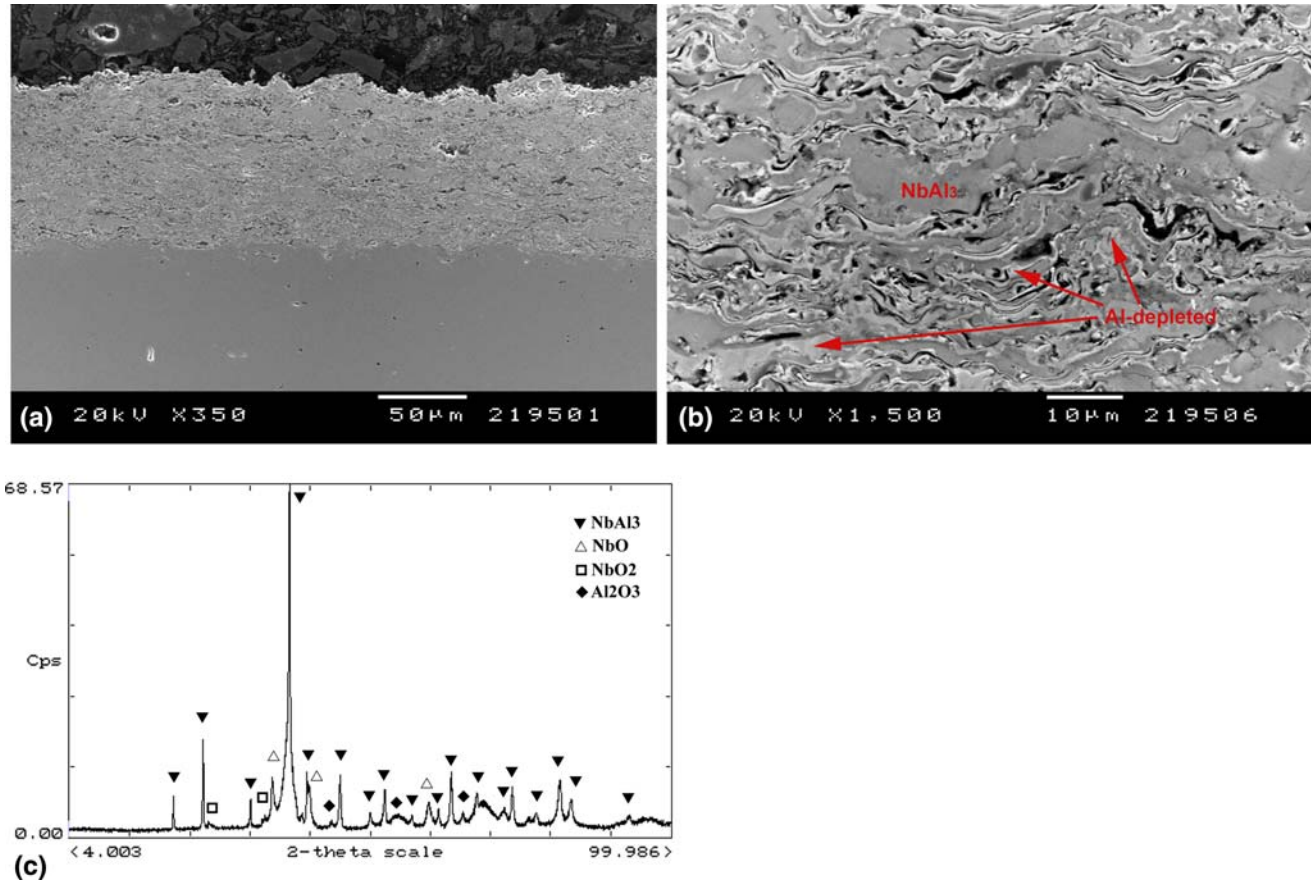

Fig. 4 (a) General view and (b) magnification of the as-sprayed cross section $NbAl_3$ coating, and (c) x-ray spectrum

Table 2 Coating features

	% Oxidation	% Porosity
FeAl	13.4 ± 2.6	1.8 ± 0.1
$NbAl_3$	13.2 ± 1.9	3.2 ± 0.9

Table 3 Abrasive wear rates

	Abrasive wear rate, $mm^3/N\ m$
Fe40Al	3.7×10^{-5}
$NbAl_3$	1.2×10^{-4}

Table 2 includes a description of the main features of the sprayed coatings such as oxidation and porosity. In a previous study, different conditions were tested, leading to the conclusion that these were close to optimum (Ref 18). The $NbAl_3$ alloy, with a higher melting point (1680 compared to 1250 °C for FeAl), required a change in the spraying parameters to a higher oxygen/fuel ratio for good efficiency. With a ratio of up to ~4.2, the propylene has a negligible cooling effect on the particles and high oxygen flux leads to considerable oxidation.

3.3 Mechanical Properties: Hardness, Friction, and Abrasive Behavior

Greater hardness for the niobium aluminide coatings was revealed by the Vickers indentation test, with an HV_{200} of 666 ± 28, whereas the iron aluminide sample had a value of 434 ± 48. The hardness is affected by all the phases included in the indentation print, which means that the 434 HV_{200} is the mean hardness for the FeAl and $FeAl_2O_4$ phases, whereas the 666 HV_{200} is the mean for $NbAl_3$, NbO, and NbO_2.

Previous thermally sprayed FeAl coatings obtained by other authors reached maximum hardnesses of 520 HV, because of the lower porosity and oxidation produced by spraying at the highest particle velocities (Ref 20, 21). Although the comparison of two different techniques may not be fully justified, as a reference, a recent study reported the formation of a niobium aluminide overlay using a plasma transferred arc welding process (PTA). This welding process produces dense coatings with a high influence of dilution, that is, the participation of the substrate in the coating alters its chemical composition (Ref 22). Analysis of different intermetallic Ni-Al, Fe-Al, and Nb-Al mixtures revealed greater hardness for the niobium aluminide coating produced from the richer Al (40 wt.%) powder, which had an HV of over 620. It also exhibited the highest abrasive resistance, as abrasive damage is normally dependent on material hardness (Ref 23). However, Table 3 shows that despite being

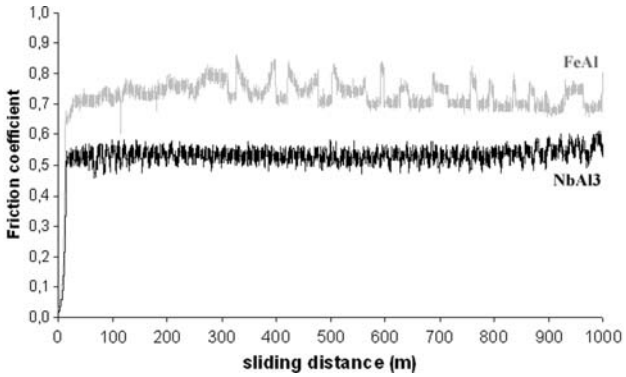

Fig. 5 Friction coefficient of iron- and niobium aluminide coatings

Table 4 Friction wear rates

	Wear rate, mm^3/Nm
Fe40Al	5.9×10^{-6}
$NbAl_3$	3.6×10^{-4}

harder, the niobium aluminide coating had the lowest abrasive resistance. One possible explanation for this is that so much oxidation at the interlamella boundaries produced an embrittlement effect which could favor crack nucleation and the detachment of particles rather than plastic deformation. The ball-on-disc tests showed that the iron aluminide coating possessed a higher friction coefficient (Fig. 5), but lower wear rate (Table 4). This could be explained by assuming that the embrittlement effect associated with intersplat oxidation explained above, facilitates the delamination mechanism by which the material is removed. The examination of the wear tracks shows that iron aluminide debris is formed of plate-like shapes corresponding to oxidized areas (Fig. 6a), whereas the niobium aluminide coating shows scratch wear scars with some fractured regions (Fig. 6b). Thus, FeAl shows a mainly adhesive mechanism, but instead of forming a transfer layer on the ball, the wear debris is removed to the edges of the wear track. In contrast, the morphology of the niobium aluminide wear track seems to have resulted from an abrasive mechanism, which is possible if wear debris remains between the two surfaces, producing a third-body abrasion effect. The influence of these removed particles however, normally causes a rise in friction coefficient and wear rate. In this case, the wear rate is comparatively higher for the niobium aluminide than for the iron aluminide coating, but the friction coefficient is lower; thus, it is difficult here to ensure that such behavior is mostly influenced by the material chemical composition or the structure of the coating.

3.4 Oxidation Performance

Figure 7 shows the heat flow and mass gain-temperature dependence for the as-sprayed coatings during the

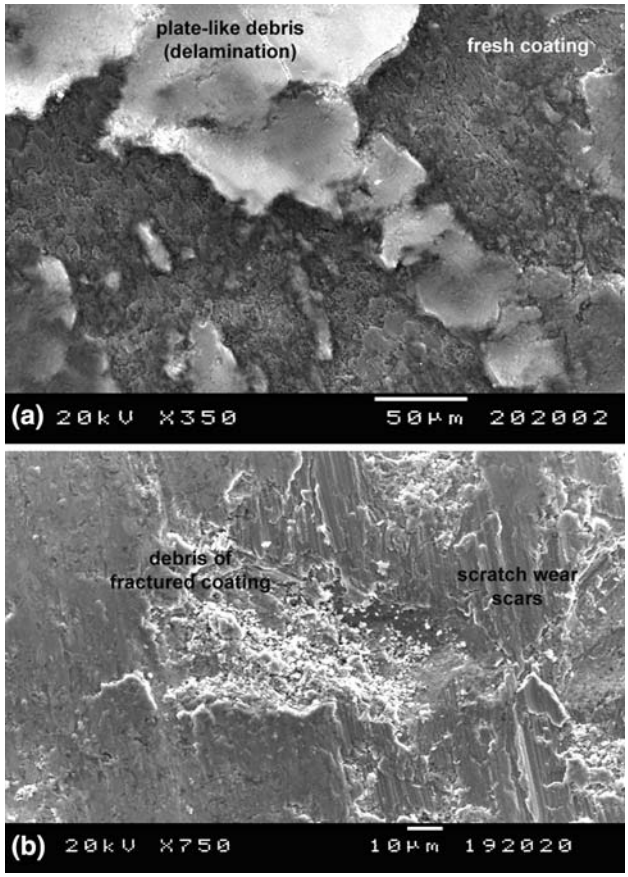

Fig. 6 Debris morphologies on the wear track of (a) iron- and (b) niobium aluminide coatings

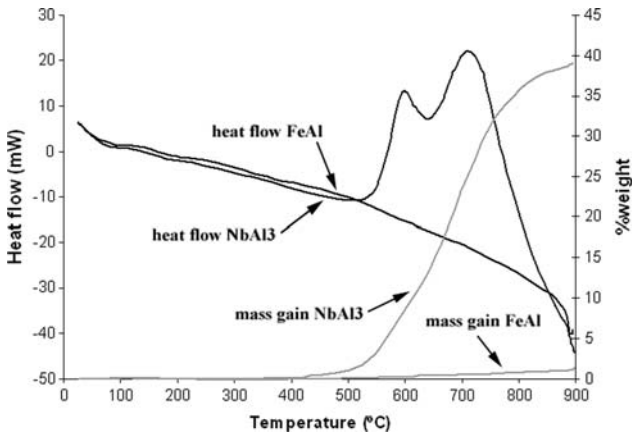

Fig. 7 Heat flow and mass gain-temperature dependence for the continuous oxidation of the as-sprayed coatings

oxidation test in a DTA-TGA equipment. While the weight of the iron aluminide coating increases continuously as a result of oxidation, without any change in the heat flow curve, the niobium aluminide coating gains considerable weight at the same time as there is a change in the heat flow curve. The two overlapping peaks, with

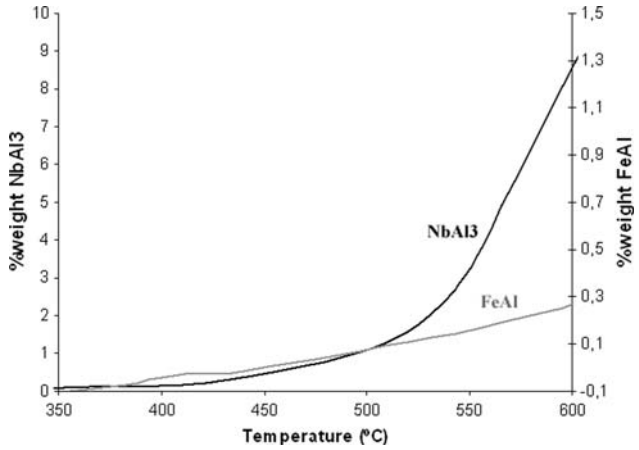

Fig. 8 Magnification of the DSC-TGA measurements within the temperature range 350-600 °C

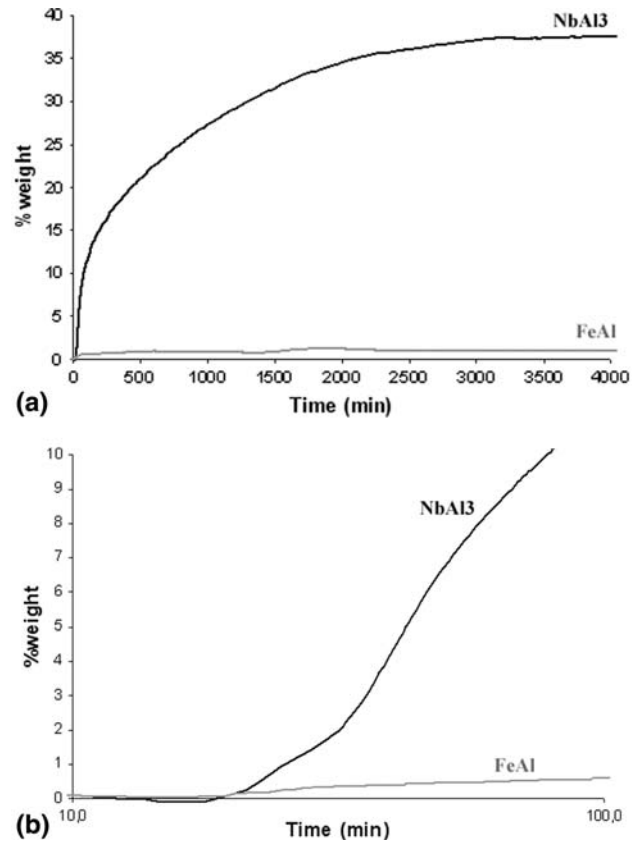

Fig. 9 Comparison of the mass change of the iron- and niobium aluminide specimens during isothermal oxidation test at 500 °C for 72 h: (a) linear and (b) logarithmic scale

peak temperatures of approximately 595 and 710 °C, correspond to severe oxidation processes; the final product is a white powder-like material. As the enlargement in Fig. 8 shows, the curve of the as-sprayed Fe40Al is an approximately linear function, while $NbAl_3$ shows more complex behavior: there is an initial linear stage from 400

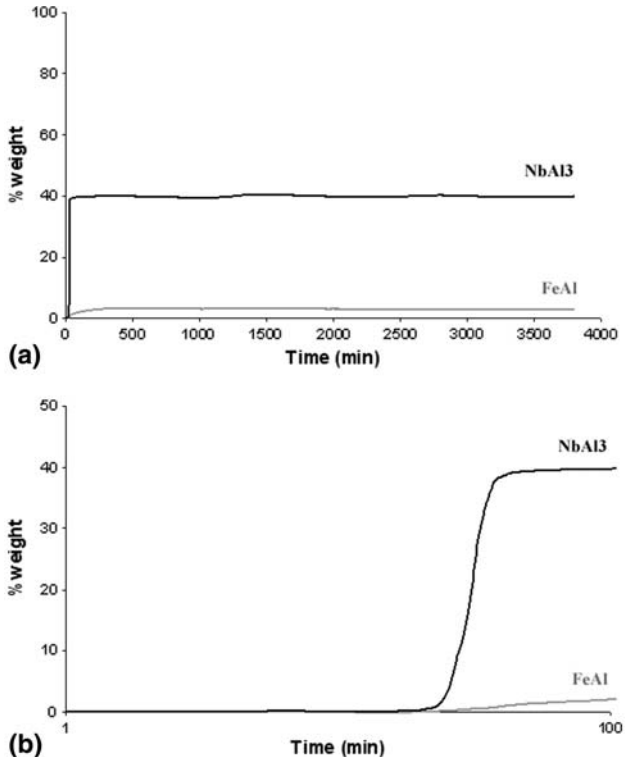

Fig. 10 Comparison of the mass change of the iron- and niobium aluminide specimens during isothermal oxidation test at 900 °C for 72 h: (a) linear and (b) logarithmic scale

to 500 °C followed by an almost exponential function, suggesting that different oxidation mechanisms are at work above and below 500 °C.

As a result of such observations, temperatures of 500 and 900 °C were chosen for the isothermal oxidation measurements, in order to study the kinetics of the medium- and high-temperature oxidation processes separately. The results of these measurements are shown in Fig. 9 and 10. Fairly logarithmic-like behavior can clearly be seen at 500 °C for the niobium aluminide coating (Fig. 9). The logarithmic-scale plot shows that the main oxidation at 500 °C starts after only about 20 min and that after approximately 30 min the rate of oxidation accelerates. This acceleration continues until about 3,000 min, when near saturation level is reached. At 900 °C (Fig. 10), the iron aluminide coating shows a logarithmic oxidation rate that increases its weight asymptotically up to approximately 3% during the first 360 min (6 h), after which time its weight remains almost constant. In contrast, the as-sprayed $NbAl_3$ attains a 40 wt.% increase in the first hour. With the logarithmic scale, one can see that both layers start to oxidize after about 20 min, but the $NbAl_3$ increases sharply from 20 to 50 min, beyond which time it stabilizes. This time range corresponds to the heating step ramp at the interval from 400 to 900 °C, where it was already observed that it suffered from pesting (Ref 24, 25).

Both iron and nickel aluminides have very different oxidation mechanisms from those of refractory metal compounds such as $MoSi_2$ or $NbAl_3$. In Ni- and Fe-based

compounds with high Al content, the formation of oxides that are thermodynamically less stable but which grow more rapidly is prevented by a protective alumina layer. Nevertheless, it should be borne in mind for Nb- and Ti-based systems that: (1) the base metal oxides (NbO_2 and TiO_2) are of comparable stability to alumina and have much higher growth rates than do NiO or FeO, making the formation of a homogeneous Al_2O_3 layer difficult; and (2) whenever the activity of Al is reduced, the stability of the oxide scale is diminished considerably. In particular, $NbAl_3$ and $MoSi_2$ (Ref 26) show linear Nb and Mo oxidation kinetics, and thus tend to lead to the removal of any protective oxide nuclei. In addition, $NbAl_3$ and $MoSi_2$, unlike $TiAl_3$, exist in a narrow composition range, so that a lower stoichiometric phase is formed beneath the oxide in the Al- or Si-depleted zone, and this influences the subsequent stability and adherence of the protective oxide.

A previous study of FeAl coatings examined the oxidation properties of iron aluminide coatings at 900, 1000, and 1100 °C (Ref 27). Oxidation at 900 °C featured the formation of a layered oxide scale consisting of a thin alumina layer and the formation of transient oxides on the top; e.g., $FeAl_2O_4$ and Fe_2O_3. This behavior is normally observed when Al concentration is low and the alumina is formed as the internal oxide precipitates: thus it offers no protection and allows the formation of rapidly growing iron oxide. However, as the oxide scale was fairly dense, oxidation resistance was reasonably high. Such an interpretation of the oxidation mechanism within the coating is based on the assumption that the powder becomes Al-depleted as the coating builds up and that internal coating defects act as additional paths for ion diffusion. The only problems then reported for the iron aluminide coating in terms of its oxidation resistance at 900 °C depend on the oxide scale adherence. The degree of spallation will therefore determine the oxidation rate. Above 1000 °C, however, although the formation of a compact adherent α-alumina scale is reported for bulk materials, intrinsic Al depletion within the as-sprayed coating becomes critical and the presence of voids at the coating-oxide scale interface, as well as the mismatch of expansion coefficients, are the sources of poor adherence and the trigger for rapid oxidation.

The oxidation of the niobium aluminide-coated specimen at 500 °C yielded a light gray powder-like material, similar to that observed after the TGA experiment, thus indicating that oxidation had already begun. When the temperature was increased to 900 °C, the coating transformed into a thick white brittle layer, showing that $NbAlO_4$, critical for pesting, had formed. This was confirmed by XRD (Fig. 11a). It is worth noting the formation of Nb_2O_5 with a Pilling-Bethworth relationship of 2.68, which makes it a nonprotective oxide. Then, when the scale was smashed, iron oxides were also detected (Fig. 11b), indicating that the steel substrate had oxidized beneath the coating; this might be due to the mismatch of thermal expansion coefficients. The top surface included a powder Nb-based morphology (Fig. 12a and c) as well as the formation of some porous iron niobium oxide nodules and needle-like oxides typical of NbO_z (Fig. 12b and d)

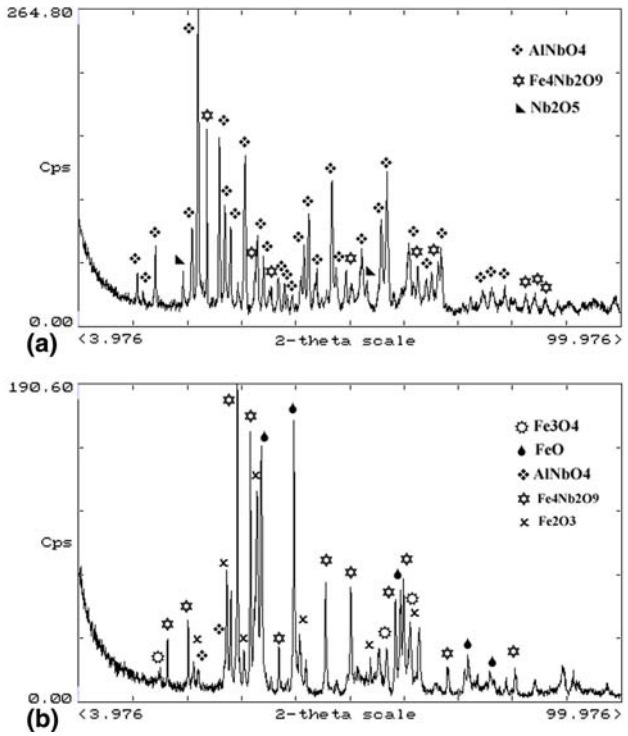

Fig. 11 XRD spectra of the (a) top surface and (b) smashed oxide scale of the niobium aluminide coating after oxidation for 72 h at 900 °C in an air atmosphere

(Ref 28). These iron niobium oxides, not observed at 500 °C, might be formed by outward Fe diffusion. Finally, the difference in the expansion coefficients induced the detachment of the oxide scale.

When the Nb-Al coated sample was tested for 1 h in the same oxidizing atmosphere at 900 °C, the scale was thinner and completely white, also with a powder-like morphology and with no signs of iron niobium oxides (as there had been in the oxidation at 500 °C). By contrast, the experiment with a continuous argon flux did not even show that the coating turned white: it still conserved its dark gray color. It does not mean, however, that the material has not been oxidized since the x-ray (Fig. 13) showed the beginning of the oxidation process marked by the presence of $NbAlO_4$ and $Fe_4Nb_2O_9$. This indicates that the remaining atmospheric oxygen content, though small, had already caused slight oxidation.

The formation of $NbAlO_4$ (Fig. 14a) is a critical step which occurs even more readily in the oxidation of the coating than a niobium aluminide bulk material, because the coating is not solely composed of the $NbAl_3$ ''line compound.'' As a consequence, Nb-Al binary compounds with lower stoichiometry such as Nb_2Al, appear in the subsurface, and these tend to produce cracking as can be observed in Fig. 14(b). This causes further oxygen penetration that in turn oxidizes the lower aluminide rapidly (Ref 29, 30). At the same time as this happens, there is an outward diffusion of Fe that combines with niobium to form mixed oxides and an inward penetration of oxygen that results in corrosion of the steel substrate.

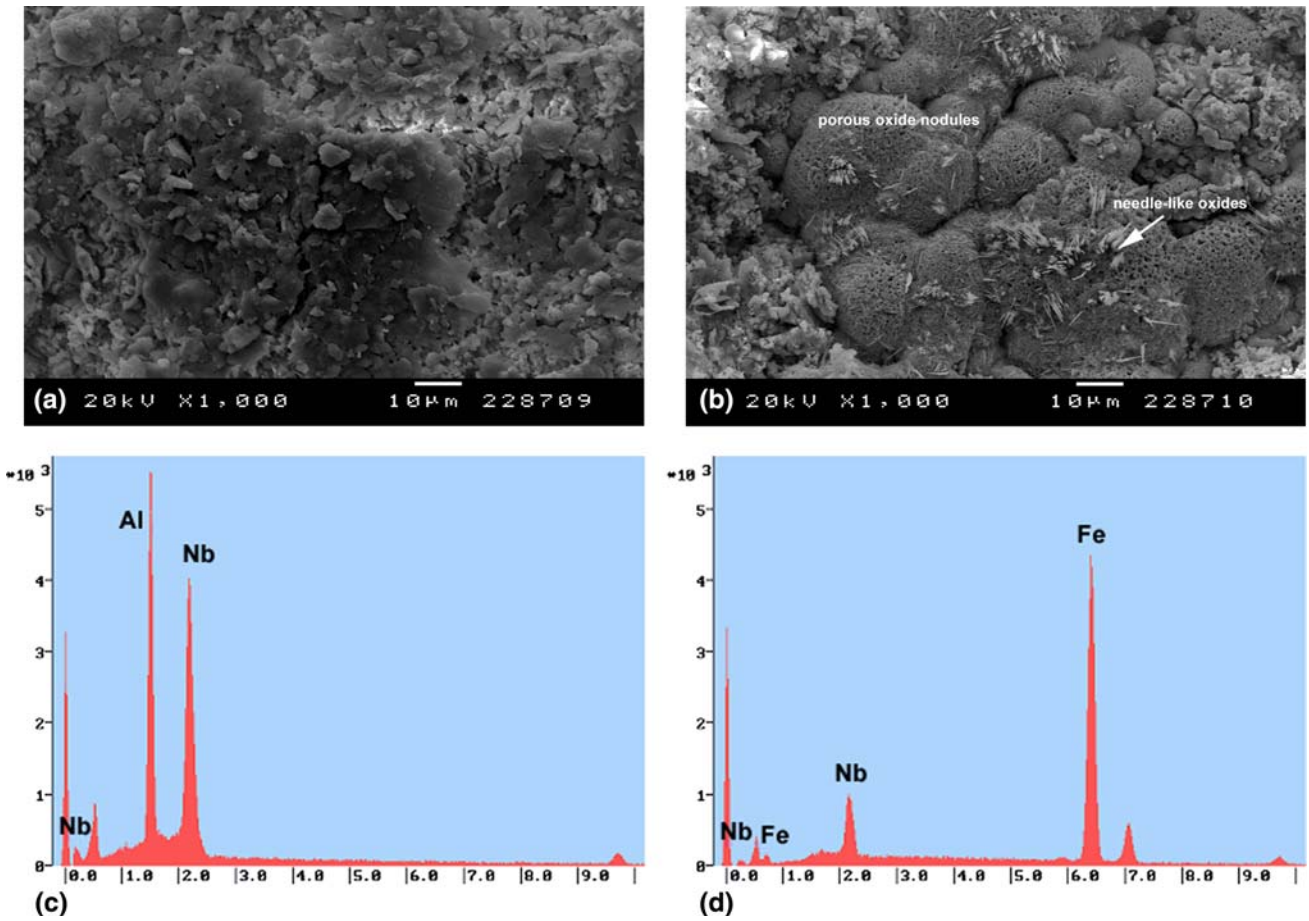

Fig. 12 (a, b) Oxide morphologies on the top surface of the oxidized niobium aluminide coating for 72 h at 900 °C in an air atmosphere and (c, d) their respective EDS microanalysis

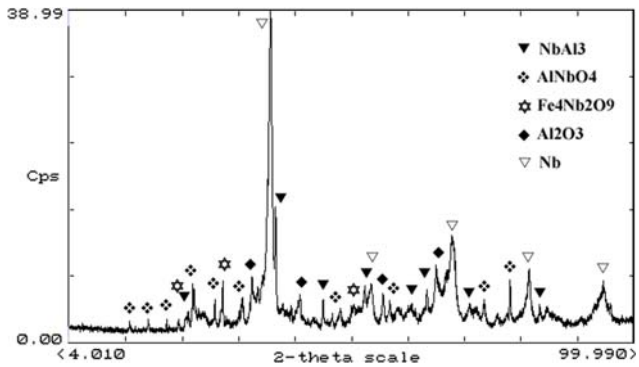

Fig. 13 XRD spectrum of the niobium aluminide coating after oxidation under low oxygen pressure conditions for 1 h at 900 °C

4. Conclusions

Both iron and niobium aluminide coating have been obtained by HVOF after optimization of the spraying parameters in the attempt to achieve the lowest oxidation content as possible.

Due to the feedstock powder characteristics, HVOF spraying leads to significantly different coating microstructures; therefore, it is difficult to compare how they will behave in similar conditions since the evaluation cannot be just done in terms of chemical composition but also coating features.

In view of the previous results, the iron aluminide coating performs better than the $NbAl_3$. Whether in the wear or the oxidation tests, niobium aluminide suffers more damage and fails earlier:

- The explanation for the poorer abrasion wear properties may be related to the structure of the coating itself, rather than to the material composition, as the material possesses much greater hardness, which is usually related to increased wear resistance. The main mechanism, by which further damage is caused in the niobium coatings, is thought to be a brittle effect that leads to interlamellar cracking and easy decohesion. On the other hand, the explanation for the sliding wear performance seems not to be clear.
- Finally, the oxidation analysis reveals that despite the high melting point of $NbA1_3$, it suffers from pesting (intergranular disintegration) at moderate temperatures.

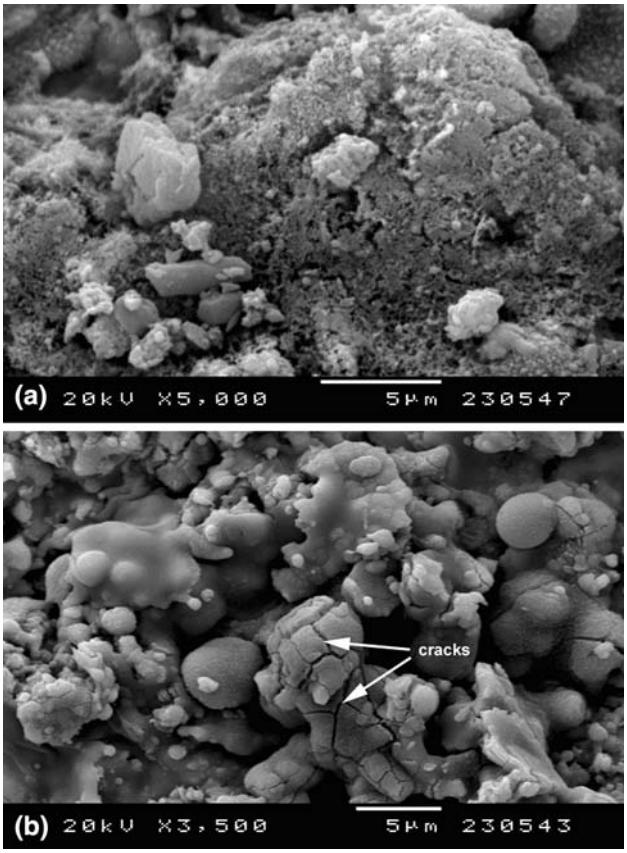

Fig. 14 (a, b) Oxide morphologies on the top surface of the niobium aluminide coating after oxidation under Ar flow at 900 °C for 1 h

This is favored by the high level of oxidation and coating defects that facilitate oxygen diffusion inwards and Al-depletion in the as-sprayed coating itself.

Acknowledgments

N. Cinca would like to thank the Generalitat de Catalunya, project 2005SGR00310 and the Ministerio de Educación y Ciencia, project MAT2006-06025 and research grant AP-2004-2453, for their economic support.

References

1. J.H. Westbrook, Applications of Intermetallic Compounds, *MRS Bull.*, 1996, **21**(5), p 26-28
2. S.C. Deevi, V.K. Sikka, and C.T. Liu, Processing, Properties and Applications of Nickel and Iron Aluminides, *Progr. Mater. Sci.*, 1997, **42**, p 177-192
3. E.P. George, M. Yamaguichi, K.S. Kumar, and C.T. Liu, Ordered Intermetallics, *Annl Rev. Mater. Sci.*, 1994, **24**, p 409-451
4. C.T. Liu, J. Stringer, J.N. Mundy, L.-L. Horton, and P. Angelini, Ordered Intermetallic Alloys: An Assessment, *Intermetallics*, 1997, **5**, p 579-596
5. C.T. Liu and J.O. Stiegler, Ductile Ordered Intermetallic Alloys, *Science*, 1984, **226**, p 636-642
6. H. Skoglund, M. Knutson, and B. Karlsson, Processing of Fine-Grained Mechanically Alloyed FeAl, *Intermetallics*, 2004, **12**, p 977-983
7. I. Baker, P. Nagpal, F. Liu, and P.R. Munroe, The Effect of Grain Size on the Yield Strength of FeAl and NiAl, *Acta Metall. Mater.*, 1991, **39**(7), p 1637-1644
8. D.G. Morris and M.A. Morris-Muñoz, The Influence of Microstructure on the Ductility of Iron Aluminides, *Intermetallics*, 1999, **7**, p 1121-1129
9. G.H. Bozzolo, R.D. Noebe, and C. Amador, Site Occupancy of Ternary Additions to B2 Alloys, *Intermetallics*, 2002, **10**, p 149-159
10. A.O. Mekhrabov and M.V. Akdeniz, Effect of Ternary Alloying Elements Addition on Atomic Ordering Characteristics of Fe-Al Intermetallics, *Acta Mater.*, 1999, **47**(7), p 2067-2075
11. C.T. Liu, E.P. George, P.J. Maziasz, and J.H. Scneibel, Recent Advances in B2 Iron Aluminide Alloys: Deformation Fracture and Alloy Design, *Mater. Sci. Eng. A*, 1998, **258**, p 84-98
12. J.H. Schneibel, E.P. George, and I.M. Anderson, Tensile Ductility, Slow Crack Growth, and Fracture Mode of Ternary B2 Iron Aluminides at Room Temperature, *Intermetallics*, 1997, **5**, p 185-193
13. C.L. Fu and J. Zou, Site Preference of Ternary Alloying Additions in Feal and NiAl by First-Principles Calculations, *Acta Mater.*, 1996, **44**(4), p 1471-1478
14. T. Tabaru and S. Hanada, High Temperature Strength of NbsAl-Base Alloys, *Intermetallics*, 1998, **6**, p 735-739
15. S. Hanada, Niobium Aluminides, *Curr. Opin. Solid State Mater. Sci.*, 1997, **2**(3), p 279-283
16. www.cbmm.com.br/portug/sources/techlib/science_techno/table_content/sub_3/images/pdfs/016.pdf
17. V. Gauthier, F. Bernard, E. Gaffet, Z.A. Munir, and J.P. Larpin, Synthesis of Nanocrystalline $NbAl_3$ by Mechanical and Field Activation, *Intermetallics*, 2001, **9**, p 571-580
18. J.M. Guilemany, N. Cinca, C.R.C. Lima, and J.R. Miguel, Studies of Fe40Al Coatings Obtained by High Velocity Oxy-Fuel, *Surf. Coat. Tech.*, 2006, **201**, p 2072-2079
19. B.D. Cullity, *Elements of X-ray diffraction*, 2nd ed., Addison-Wesley, cop. 1978
20. T. Totemeier, R. Wright, and W.D. Swank, FeAl and Mo-Si-B Intermetallic Coatings Prepared by Thermal Spraying, *Intermetallics*, 2004, **12**, p 1335-1344
21. G. Ji, T. Grosdidier, H.L. Liao, J. Morniroli, and C. Coddet, Spray Forming Thick Nanostructured and Microstructured FeAl Deposits, *Intermetallics*, 2005, **13**, p 596-607
22. A. D'Oliveira, A. de Christo, D. S. Vaz, and B. R. Curitiba, Evaluation of Intermetallic Coatings Processed by PTA, *International Thermal Spray Conference 2008*, Maastricht
23. I.M. Hutchings, Tribology: Friction and Wear of Engineering Materials, *A Division of Hodder Headline PLC*, E. Arnold, Ed., 1992, p 103-105, ISBN 0-340-56184-x
24. G. Raisson and A. Vignes, Oxidation and the Phenomenon of Catastrophic Deterioration of Niobium Aluminide $NbAl_3$, *Revue de Physique Appliqque*, 1970, **5**, p 535
25. S.V. Raj, M. Hebsur, E. Locci, and J. Doychak, Effect of Oxidation on the Mechanical Properties of a $NbAl_3$ Alloy at Intermediate Temperatures, *Mater. Res. Soc.*, 1992, **7**(12), p 3219-3234
26. T.A. Kircher and E.L. Courtright, Engineering Limitations of $MoSi_2$ Coatings, *Mater. Sci. Eng. A*, 1992, **155**, p 67-74
27. J.M. Guilemany, N. Cinca, S. Dosta, and C.R.C. Lima, High Temperature Corrosion of Fe-40Al Coatings, *Intermetallics*, 2007, **15**, p 1384-1394
28. W.M.M. Huijbregts, and M.J. Brabers, Oxidation of Niobium Coated with Aluminium in Steam-Air Mixtures, *J. Intern d'étude sur l'Oxydation des Metaux*, 1965, p 61-69, http://www.hbscc.nl/pdf/01%20Niobium.pdf
29. G.H. Meier, Research on Oxidation, Embrittlement of Intermetallic Compounds in the U.S, *Mater. Corros.*, 1996, **47**, p 595-618
30. V. Gauthier, C. Josse, J.P. Larpin, and M. Vilasi, High-Temperature Oxidation Behavior of the Intermetallic Compound $NbAl_3$: Influence of Two Processing Techniques on the Oxidation Mechanism, *Oxidat. Metal*, 2000, **54**(1/2), p 27-45